

On origami-like quasi-mechanisms with an antiprismatic skeleton

G. Nawratil

*Institute of Discrete Mathematics and Geometry & Center for Geometry and Computational Design, TU Wien, e-mail:
nawratil@geometrie.tuwien.ac.at*

Abstract. We study snapping and shaky polyhedra which consist of antiprismatic skeletons covered by polyhedral belts composed of triangular faces only. In detail, we generalize Wunderlich's trisymmetric sandglass polyhedron in analogy to the generalization of the Jessen orthogonal icosahedron to Milka's extreme birosette structures, with the additional feature that the belt is developable into the plane as the Kresling pattern. Within the resulting 2-dimensional family of origami-like sandglasses we study the 1-parametric sets of quasi-mechanisms which are either *shaky* or have an *extremal snap*, i.e. one realization is on the boundary of self-intersection. Moreover, we evaluate the capability of these snapping/shaky quasi-mechanisms to flex on base of the *snappability* index and the novel *shakeability* index, respectively.

Key words: model flexors, quasi-mechanisms, snapping, shakiness, snappability, shakeability, origami

1 Introduction

We consider polyhedral structures, where the bottom face α and the parallel top face β are regular convex n -gons A_0, \dots, A_{n-1} (with center A) and B_0, \dots, B_{n-1} (with center B), respectively, for $n \geq 3$ and a side length of 1. Moreover, these two faces are twisted against each other by a rotation about the orthogonal axis AB (cf. Fig. 1a). Then this antiprismatic skeleton is covered by a polyhedral belt composed of triangular faces only. Moreover, all resulting polyhedra discussed in the paper do not possess continuous isometric deformations; i.e. they are rigid from the mathematical point of view. But the physical models of these polyhedra can flex due to non-destructive elastic deformations of material (or backlash/tolerances in hinges), i.e. small changes in the intrinsic metric (given by the edge lengths) have significant effects on the spatial shape. Therefore these structures are also known as *model flexors* or *quasi-mechanisms*.

If the inner geometry (intrinsic metric together with the combinatorial structure) of the polyhedron is fixed, then the embedding of the polyhedron into the Euclidean 3-space E^3 is in general not uniquely determined; i.e. the polyhedron has different



Fig. 1 The antiprismatic skeleton for $n = 3$ (a), its belt given by the Kresling pattern (b), the resulting octahedral structure (c) and its configuration after the snap (d).

incongruent realizations¹. Based on these basic notations we can distinguish the following two kinds of quasi-mechanisms:

- (i) Snapping quasi-mechanism: The shape variation results from the snap (caused by deformation) of a given realization into another one. An example for this is the Siamese dipyrmaid, which even snaps between three realizations [2, 9].
- (ii) Shaky quasi-mechanism: Now the deformed states originate from a given *shaky* (also known as *singular* or *infinitesimal flexible*) realization. The best known example for this kind of model flexion is the Jessen orthogonal icosahedron [6, 2, 3] (cf. Fig. 2a). Note that shakiness can be seen as the limit of snapping when the related realizations converge to coincidence [11, 9].

There are also examples, like the four-horn [15, 9], which use both functional principles (i & ii) at the same time.

Review. We proceed with a review on model flexors with an antiprismatic skeleton:

- (1) Let us start with the Kresling pattern [7], a flat strip of congruent triangles (cf. Fig. 1b) which can be folded up and closed to a belt for the skeleton. The resulting antiprismatic structure has a bi-stable behavior, which was already known to Wunderlich (cf. [13] and for $n = 3$ the more detailed study [12]). During the snap, the relative motion of α and β is composed of a rotation about AB and a change in height (see Fig. 1c,b). A detailed literature review on these structures (as well as a study of related ones) is given by the author in [10].
- (2) Next, we consider so-called extreme birosettes [4], which can be seen as generalizations of the Jessen orthogonal icosahedron (case $n = 3$). In this case the belt consists of $2n$ equilateral triangles with side length of 1 and $2n$ petals, which are skew rhombi of side length 1 broken along one of its diagonals² of length p . The resulting structure is symmetric with respect to (a) rotations of $\frac{2\pi}{n}$ about AB and (b) a reflection at the birosette center (midpoint of AB) which has to be complemented by a rotation of $\frac{\pi}{n}$ about AB for even values of n (see Figs. 2a and 3). The relative instantaneous motion of α and β is translatory in direction of AB . Moreover, the maximal value p_+ of p such that the birosette can be assembled under consideration of the mentioned symmetry, yields the *extreme* birosette. Note that birosettes for $n = 3$ are also known as Douady shaddocks [1, 3].

¹ In this paper the word realization always refers to an undeformed embedding into E^3 .

² Note that the birosette degenerates into an antiprism if p converges towards zero.

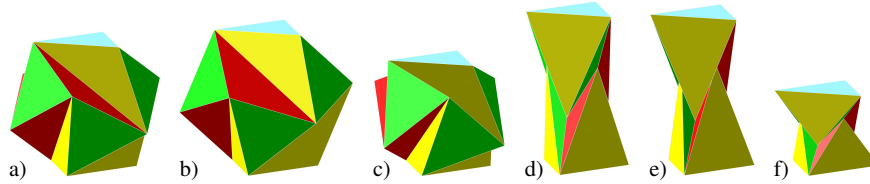


Fig. 2 (a) Jessen orthogonal icosahedron [6], (b,c) two snapping realizations of a non-extremal birosette for $n = 3$ with $p = 1.6 < p_+ = 4/\sqrt{6}$, (d,e) the two realizations of the snapping sandglass icosahedron of Wunderlich [14, Fig. 6], (f) shaky sandglass icosahedron [14, Fig. 4].

- (3) Finally, we recall Wunderlich’s trisymmetric sandglass polyhedron [14], which is a snapping icosahedron possessing the same symmetry and combinatorial structure as the birosette for $n = 3$. In this case the belt consists of six congruent isosceles triangles, whose bases of length 1 are hinged to the equilateral triangles α and β , respectively, and the gaps between them are filled by further 12 congruent isosceles triangles (see Fig. 2d,e). During the snap, the relative motion of α and β is a translation along AB .

Remark 1. By considering the limit mentioned in (ii) one can also produce shaky quasi-mechanisms from the snapping structures given in (1) studied in [13, 12] and (3) illustrated in Fig. 2f. Also snapping birosettes can be generated by choosing $p < p_+$ as displayed in Fig. 2b,c. \diamond

Outline. Based on this review we generalize Wunderlich’s sandglass polyhedron to arbitrary n in analogy to the birosette construction, with the additional feature that the belt is developable into the plane as the Kresling pattern (cf. Section 2), which allows an efficient production. Within the resulting 2-dimensional family of origami-like sandglasses (for arbitrary $n \geq 3$) we study the 1-parametric sets of quasi-mechanisms which are either *shaky* (cf. Section 4) or have an *extremal snap* (cf. Section 3), i.e. one realization is on the boundary of self-intersection. Moreover, in these two sections we also evaluate the capability of these snapping/shaky quasi-mechanisms to flex on base of the *snappability* index (cf. [8, 9]) and the novel *shakeability* index, respectively. The paper is concluded in Section 5.

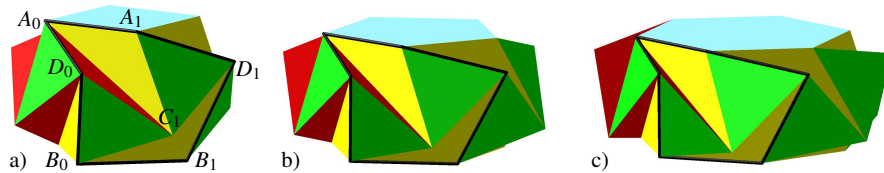


Fig. 3 Extreme birosettes for $n = 4, 5, 6$ (a,b,c) with yellow/red pedals, where the unit-cells are framed in black.

2 Preliminary considerations

Assume that we have given a polyhedron with the combinatorial structure of a birossette for arbitrary $n \geq 3$. In order to clarify its degree of freedom (dof), we use the notation of Fig. 3a, where the vertices of a unit-cell³ of the belt are labeled. The relative position of β with respect to α has 6 dofs and each vertex C_i and D_i has further 3 dofs, which yields in total $6 + 6n$ dofs. Moreover, we have $8n$ distance constraints implied by the edges of the structure, with exception of those belonging to the skeleton. Therefore the dof of the structure is computed by $F := 6(n+1) - 8n$ yielding for $n \geq 3$ a value of $F \leq 0$, which shows that these structures are in general rigid⁴.

Remark 2. It is an open question whether flexible polyhedrons exist having the same combinatorial structure as a birossette with $n \geq 3$. \diamond

The assumptions on the edge lengths (inside a unit-cell) of a birossette can be weakened as follows without destroying its symmetry:

$$L_1 := \overline{B_0D_0} = \overline{A_1C_1}, \quad L_2 := \overline{B_0C_1} = \overline{A_0D_0}, \quad L_3 := \overline{D_0C_1} = \overline{C_1D_1}, \quad L_4 := \overline{B_0D_1} = \overline{A_0C_1} \quad (1)$$

beside the unit length of $\overline{A_0A_1}$ and $\overline{B_0B_1}$. Moreover, in the remainder of the paper we assume that these skeleton edges are undeformable under the model flexibility in contrast to the other edge lengths $L_1, \dots, L_4 > 0$, which can vary⁵.

One can compute (cf. Appendix 5.1 for details) the condition for the developability of the obtained generalized birossette belt in terms of L_1, \dots, L_4 . Under consideration of the sandglass condition $L_1 = L_4$ this origami condition reads as:

$$Q_3 = Q_1 + Q_2 - \sqrt{Q_2(4Q_1 - 1)} \quad \text{with} \quad Q_i := L_i^2 \quad (2)$$

Remark 3. Wunderlich further assumed in the study of the trisymmetric sandglass [14] that $L_2 = L_3$ holds, which simplifies the related equations considerably and allows a very compact treatment. We do not make this assumption here. \diamond

3 Snapping quasi-mechanisms

As the generalized Wunderlich sandglasses have the same symmetry as the birossettes, the essential vertices of the unit-cell can be coordinatized similarly to [4] by

$$A_0 = (R, 0, H), \quad B_0 = (Rc, Rs, -H), \quad D_0 = (r, 0, -h), \quad C_1 = (rc, rs, h),$$

³ A repetitive rotation of the unit-cell around the axis AB about the angle $\frac{\pi}{n}$ generates the polyhedral belt and increases the indices of the vertices by one (mod n).

⁴ Note that taking the symmetry of the birossette into account yields $F = 0$ for all $n \geq 3$.

⁵ Note that the study [4] on birossettes is more restrictive as only the length p of the diagonal is allowed to change.

using the abbreviations $c := \cos \frac{\pi}{n}$ and $s := \sin \frac{\pi}{n}$, respectively. Moreover, R equals $\frac{1}{2s}$ due to the unit-length of the skeleton edges. With this parametrization we only remain with the following three equations:

$$q_1 : Q_1 - \overline{B_0D_0}^2 = 0, \quad q_2 : Q_2 - \overline{B_0C_1}^2 = 0, \quad q_3 : Q_3 - \overline{D_0C_1}^2 = 0, \quad (3)$$

as the fourth one, namely $Q_4 - \overline{B_0D_1}^2 = 0$, is identical with q_1 . Thus for a given set of sward edge lengths Q_1, Q_2, Q_3 the corresponding realizations can be computed by solving q_1, q_2, q_3 for H, h, r , which is straight forward.

As already mentioned, we want to restrict to structures possessing an *extremal snap*, i.e. one realization is on the boundary of self-intersection. Such configurations are illustrated in Fig. 5 (right) and have the advantage that the self-blocking of the faces increases the structure's load carrying capacity. Moreover, the self-covered areas can be provided with holes. In this way the configuration of Fig. 5 (right) is still tight, thus it is called *closed*, in contrast to the *open* one of Fig. 5 (left). Therefore, such structures can for example be used as *pressure relief valves*.

At the closed state the points A_0, B_0, D_0, C_1 are coplanar. This is the case for $(2rs - 1)(2Hrs + h) = 0$ where the factors imply a dihedral angle of π and 0, respectively, along the edge D_0C_1 . Therefore we set $r = -\frac{h}{2Hs}$ and plug this expression into q_1, q_2, q_3 . By eliminating the unknowns H, r, s from these three equations together with $c^2 + s^2 - 1 = 0$ by means of resultants, we end up with

$$\begin{aligned} &4cQ_2Q_1 - 2cQ_2^2 - 2Q_1^2 - 28Q_2Q_1 - 2Q_2^2 + Q_1 + 5Q_2 - 2cQ_1^2 \\ &+ W^{3/2}\sqrt{Q_2} + 8Q_2^{3/2}\sqrt{W} + 4Q_1\sqrt{Q_2}\sqrt{W} = 0 \end{aligned} \quad (4)$$

by taking into account Eq. (2) and $W := 4Q_1 - 1$. This equation is linear⁶ in c and plotted in Fig. 4a. Moreover, it can be solved explicitly for Q_2 (e.g. with MAPLE), which yields four branches. We let Q_1 run within the interval $]0.25; 5]$ in steps of 0.01 for $n = 3, \dots, 6$ and check if this value implies a pair of snapping sandglass realizations. To do so, we compute the realizations and check in a first step if they are free of self-intersections, and in a second step if they can snap into each other by the methods presented by the author in [8, 9]. It turns out that only the branch of Eq. (4), which yields the lowest value for Q_2 carries solutions of our problem. Animations of these families of snapping sandglasses (for $n = 3, \dots, 6$) can be downloaded from the author's homepage⁷.

Snappability. According to [8, 9] the snap between two sandglass realizations has to pass a shaky configuration (with squared edge lengths S_1, S_2, S_3) at the maximum state of deformation (see Fig. 5 (center)), which is used for the evaluation of the snapping capability in terms of the *snappability*. By considering the belt as a joint-bar structure⁸ this index σ , which is based on the total elastic strain energy density of the framework, can be computed as follows (cf. [8, 9]):

⁶ For $Q_1 = Q_2$ it is independent of c but then it can only vanish for $Q_1 = Q_2 = 0$, a contradiction.

⁷ <https://www.dmg.tuwien.ac.at/nawratil/publications.html>

⁸ It can also be interpreted as a panel-hinge framework but the formula is more complicated [8, 9].

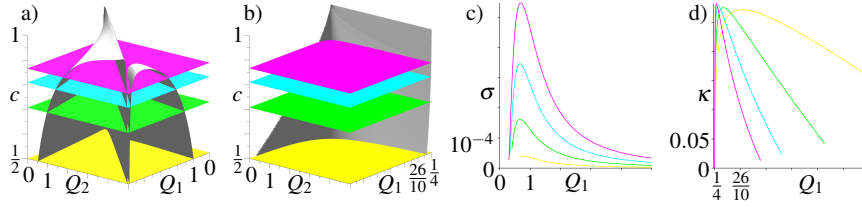


Fig. 4 Visualization of (a) Eq. (4) and (b) the shakiness condition, which only yields feasible values for Q_2 within a narrow domain of Q_1 , where $Q_1 = \frac{1}{4}$ is an asymptote for the Q_2 values. The horizontal c -planes for $n = 3, \dots, 6$ are colored in yellow, green, cyan and magenta, respectively. The same color-coding is used for the graphs of the snappability (c) and the shakeability (d).

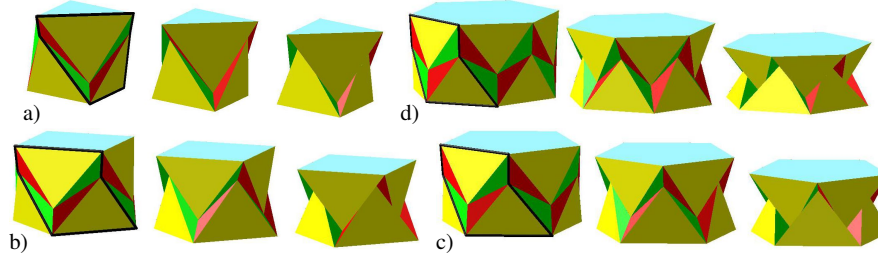


Fig. 5 Illustration of the snap from the open state (left) over the passed shaky configuration (center) to the closed state (right) for the structures causing the maximal snappability for $n = 3$ (a), $n = 4$ (b), $n = 5$ (c) and $n = 6$ (d). Moreover, the unit-cells of the open state are framed in black.

$$\sigma := \left(4n \frac{(Q_1 - S_1)^2}{8L_1^3} + 2n \frac{(Q_2 - S_2)^2}{8L_2^3} + 2n \frac{(Q_3 - S_3)^2}{8L_3^3} \right) / (4nL_1 + 2nL_2 + 2nL_3) \quad (5)$$

In Fig. 4c the snappability of the computed snapping sandglass realizations, which are free of self-intersections, are displayed. The structures causing the maximal snappability are visualized in Fig. 5. Additional graphs concerning the change in volume, height or waist radius during the snap are given in Appendix 5.4 as well as the crease pattern of the structure displayed in Fig. 5a.

4 Shaky quasi-mechanisms

For the computation of shaky origami-like sandglasses we proceed as follows. We eliminate from q_1, q_2, q_3 of Eq. (3) the unknowns H, h by means of resultant, such that we end up with a polynomial in r . In order that this polynomial has a solution of higher order, its discriminant with respect to r has to vanish. From the resulting expression we eliminate s by applying the resultant method with respect to $c^2 + s^2 - 1 = 0$. Under consideration of Eq. (2) we end up with the shakiness condition of the form $w_4c^4 + w_3c^3 + w_2c^2 + w_1c + w_0 = 0$ whose coefficients are given in Appendix 5.2 due to their length. This quartic equation in c is plotted in Fig. 4b. Note that this equation cannot be solved explicitly for Q_2 but we can evaluate it numerically.

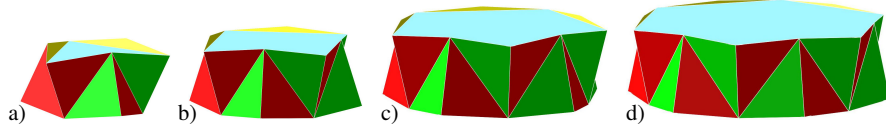


Fig. 6 Shaky structures causing the maximal shakeability for $n = 3, 4, 5, 6$ (a,b,c,d).

The shakiness of the structure is in general related with a non-trivial infinitesimal isometric deformation of dimension 1. The corresponding velocity vectors $\mathbf{v}(X_i)$ of the vertices X_i ($i = 0, \dots, n-1$) with $X \in \{A, B, C, D\}$ are determined⁹ up to a non-zero factor (fixed by Eq. (6) given later on) and can be computed by applying the *projection theorem*. For details the interested reader is referred to Appendix 5.3.

Shakeability. In order to evaluate the structure's capability to shake, we introduce the so-called *shakeability* κ , which is defined as curvature of the snappability function over the space of squared edge lengths in direction associated with the infinitesimal mobility. As the snappability function is already dimensionless we also have to normalize the velocity vectors in such a way. This can e.g. be achieved by the condition¹⁰, that the mean of the relative instantaneous changes of the squared edge lengths is equal to 1. For our sandglass structure this normalization reads as follows:

$$\left(4n \frac{\|\mathbf{v}(B_0) - \mathbf{v}(D_0)\|^2}{Q_1} + 2n \frac{\|\mathbf{v}(B_0) - \mathbf{v}(C_1)\|^2}{Q_2} + 2n \frac{\|\mathbf{v}(D_0) - \mathbf{v}(C_1)\|^2}{Q_3} \right) / (8n) = 1 \quad (6)$$

Assumed that this condition holds, we can set $S_1 = Q_1 + t\|\mathbf{v}(B_0) - \mathbf{v}(D_0)\|^2$, $S_2 = Q_2 + t\|\mathbf{v}(B_0) - \mathbf{v}(C_1)\|^2$ and $S_3 = Q_3 + t\|\mathbf{v}(D_0) - \mathbf{v}(C_1)\|^2$ and plug these expressions into Eq. (5), which now depends quadratically on t ; i.e. $\sigma(t)$. According to the well-known curvature formula the shakeability κ can then be computed as

$$\kappa := \frac{\sigma''}{(1+\sigma^2)^{3/2}} \Big|_{t=0} = \sigma'' \Big|_{t=0} \quad (7)$$

We let Q_1 run within the interval $]0.25; 0.31]$ in steps of 0.001 for $n = 3, \dots, 6$ and compute for the associated shakable realization the shakeability, which is displayed in Fig. 4d. The structures causing the maximal shakeability are visualized in Fig. 6.

Animations of the families of shakable origami-like sandglasses for $n = 3, \dots, 6$ can be downloaded from the author's homepage (cf. footnote 7) and the crease pattern of the structure displayed in Fig. 6a is given in Appendix 5.4.

Remark 4. Shakable realizations with smaller κ are more shakable, but note that the shakeability cannot vanish as in this case all the velocity vectors have to be the same; i.e. the infinitesimal isometric deformation is trivial (instantaneous translation). \diamond

⁹ Note that the faces α and β are assumed to translate instantaneously along the z -axis with the same speed but in opposite direction; i.e. $\mathbf{v}(A_i) = -\mathbf{v}(B_i)$. Therefore the symmetry of the structure remains intact by attaching the velocity vectors $\mathbf{v}(X_i)$ to the corresponding vertices X_i .

¹⁰ One can also think of other normalizations, which will effect the resulting value for κ .

5 Conclusion and future work

We generalized Wunderlich’s sandglass polyhedron in analogy to the birosette construction, with the additional feature that the belt of the antiprismatic skeleton is developable. One can think of two further generalizations of the obtained snapping or shaky quasi-mechanisms; namely (a) to omit the sandglass condition and/or the origami condition for the study of the generalized birosette structures (given by Eq. (1)) and (b) to use an antifrustum as skeleton (i.e. α and β have different radii). For the latter case one can proceed similar to [5, 10]. Moreover, we introduced the *shakeability* to evaluate the capability of a shaky quasi-mechanism to flex as counterpart to the snappability [8, 9]. As this index is dimensionless, it enables a comparison of shaky structures differing in the inner geometry, which is also subject to future research as well as the influence of the normalization condition (cf. footnote 10).

Acknowledgements The author is supported by grant P 30855-N32 of the Austrian Science Fund FWF and by FWF project F77 (SFB “Advanced Computational Design”, subproject SP7).

References

1. Douady, A.: Le shaddock à six becs. Bulletin A.P.M.E.P. **281**:699–701 (1971)
2. Goldberg, M.: Unstable Polyhedral Structures. Mathematics Magazine **51**(3) 165–170 (1978)
3. Gorkavyy, V., Kalinin, D.: On model flexibility of the Jessen orthogonal icosahedron. Beiträge zur Algebra und Geometrie **57**(3) 607–622 (2016)
4. Gor’kavyyi, V.A., Milka, A.D.: Birosettes are Model Flexors. Ukrainian Mathematical Journal **70**(7) 1022–1041 (2018)
5. Ishida, S., Nojima, T., Hagiwara, I.: Mathematical approach to model foldable conical structures using conformal mapping. Journal of Mechanical Design **136** 091007 (2014)
6. Jessen, B.: Orthogonal icosahedron. Nordisk Matematisk Tidskrift **15**(2):90–96 (1967)
7. Kresling, B.: Natural twist buckling in shells: from the Hawkmoth’s bellows to the deployable Kresling-pattern and cylindrical Miura-ori. Proceedings of the 6th International Conference on Computation of Shell and Spatial Structures (J.F. Abel, J.R. Cooke eds.), Ithaca, NY (2008)
8. Nawratil, G.: On the snappability and singularity-distance of frameworks with bars and triangular plates. In Springer’s Proceedings in Advanced Robotics of the 2nd IMA Conference on Mathematics of Robotics (2021)
9. Nawratil, G.: Snappability and singularity-distance of pin-jointed body-bar frameworks. Mechanism and Machine Theory (accepted) arXiv:2101.02490
10. Nawratil, G.: Multi-stable design of triangulated origami structures on cones of revolution. in preparation (2021)
11. Stachel, H.: What lies between rigidity and flexibility of structures. Serbian Architectural Journal **3**(2) 102–115 (2011)
12. Wunderlich, W.: Starre, kippende, wackelige und bewegliche Achtfläche. Elemente der Mathematik **20**(2) 25–32 (1965)
13. Wunderlich, W.: Snapping and Shaky Antiprisms. Mathematics Magazine **52**(4) 235–236 (1979)
14. Wunderlich, W.: Kipp-Ikosaeder II. Elemente der Mathematik **37**(3) 84–89 (1982)
15. Wunderlich, W., Schwabe, C.: Eine Familie von geschlossenen gleichflächigen Polyedern, die fast beweglich sind. Elemente der Mathematik **41**(4) 88–93 (1986)

Appendix

5.1 Origami condition for the generalized birosette belt

In this section we compute the condition for the developability of the obtained generalized birosette belt in terms of L_1, \dots, L_4 . We start with a developed unit-cell, whose vertices can be coordinatized with respect to a planar Cartesian frame as:

$$\begin{aligned} B_0^* &= (0, 0), & B_1^* &= (1, 0), & D_0^* &= (a, b), & D_1^* &= (a+1, b), \\ C_1^* &= (c, d), & A_0^* &= (a+e, b+f), & A_1^* &= (1+a+e+1, b+f), \end{aligned} \quad (8)$$

without loss of generality. Note that the repetition of the unit-cell implies the parallelism of $B_0^*D_0^* \parallel B_1^*D_1^*$ as well as $A_0^*D_0^* \parallel A_1^*D_1^*$ (cf. Fig. 7), where the upper index $*$ indicates the development. Moreover, we have to assume that $b, d, f > 0$ has to hold in order to avoid overlaps of the development. It can easily be verified that the conditions (cf. Eq. (1))

$$\overline{B_0^*D_0^*} = \overline{A_1^*C_1^*}, \quad \overline{B_0^*C_1^*} = \overline{A_0^*D_0^*}, \quad \overline{D_0^*C_1^*} = \overline{C_1^*D_1^*}, \quad \overline{B_0^*D_1^*} = \overline{A_0^*C_1^*} \quad (9)$$

imply the relations $d = f$, $e = -c$ and $c = a + \frac{1}{2}$. Now the remaining unknowns a, b, f can be expressed in terms of L_1, L_2, L_4 from

$$Q_1 - \overline{B_0^*D_0^*}^2 = 0, \quad Q_2 - \overline{B_0^*C_1^*}^2 = 0, \quad Q_4 - \overline{B_0^*D_1^*}^2 = 0 \quad (10)$$

with $Q_i := L_i^2$, which yields

$$a = \frac{Q_4 - Q_1 - 1}{2}, \quad b = \frac{1}{2} \sqrt{2Q_1 + 2Q_4 - 1 - (Q_1 - Q_4)^2}, \quad f = \frac{1}{2} \sqrt{4Q_2 - (Q_1 - Q_4)^2}$$

Plugging the obtained expressions into $Q_3 - \overline{D_0^*C_1^*}^2 = 0$ implies the origami condition in terms of squared edge lengths. This condition simplifies to Eq. (2) if one takes the sandglass condition $L_1 = L_4$ ($\Rightarrow Q_1 = Q_4$) into account.

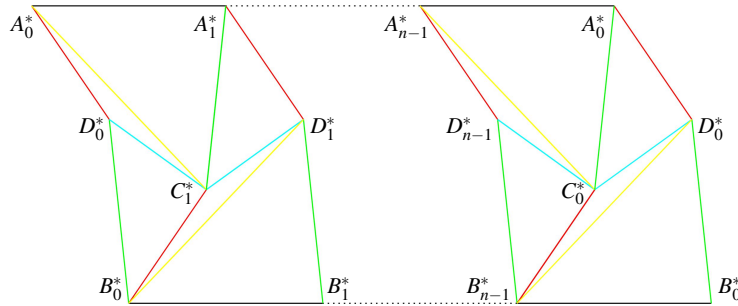


Fig. 7 Sketch for the computation of the origami condition for the generalized birosette belt. Edges with the same length are colored equally (cf. Eq. (9)).

5.2 Coefficients of the shakiness condition

The coefficients of the shakiness condition computed in Section 4 read as follows:

$$\begin{aligned}
w_4 &= 128Q_1^2Q_2^2 \\
w_3 &= \left[(64 - 96Q_1)Q_2^{5/2} - 96Q_1^2Q_2^{3/2} \right] \sqrt{W} + 64Q_1(2Q_1 - 1)Q_2^2 \\
w_2 &= 96 \left[Q_1^3 + (2Q_2 + \frac{5}{16})Q_1^2 + (Q_2^2 - \frac{23Q_2}{8})Q_1 - \frac{13Q_2^2}{48} + \frac{Q_2}{2} \right] Q_2 - \\
&\quad 48\sqrt{W}Q_1(2Q_1 - 1)Q_2^{3/2} - 24W^{3/2}Q_2^{5/2} \\
w_1 &= 96 \left[Q_1^3 + (2Q_2 - \frac{3}{4})Q_1^2 + (Q_2^2 - Q_2 - \frac{5}{32})Q_1 - \frac{Q_2^2}{4} + \frac{7Q_2}{32} \right] Q_2 - \left[8Q_2^{7/2} - \right. \\
&\quad \left. (15 + 36Q_1 - 24Q_1^2)Q_2^{3/2} + (24Q_1 + 38)Q_2^{5/2} - (2Q_1^2 - 8Q_1^3)\sqrt{Q_2} \right] \sqrt{W} \\
w_0 &= (148Q_2^2 + 35Q_2)Q_1 + 2Q_2^3 - 37Q_2^2 - Q_2 - 70Q_1^2Q_2 - \left[8Q_2^{7/2} + \right. \\
&\quad \left. (24Q_1^2 - 12Q_1 + 24)Q_2^{3/2} + 6WQ_2^{5/2} + (8Q_1^3 - 6Q_1^2 + Q_1)\sqrt{Q_2} \right] \sqrt{W}
\end{aligned} \tag{11}$$

5.3 Computing the infinitesimal motion

From item (3) of the review part and under consideration of footnote 9, the velocity vectors of A_i and B_i can be given as:

$$\mathbf{v}(A_i) = (0, 0, z), \quad \mathbf{v}(B_i) = (0, 0, -z). \tag{12}$$

Moreover, due to the symmetry of the structure we can set $\mathbf{v}(D_0) = (u, 0, v)$ ($\Rightarrow \mathbf{v}(C_1) = (uc, us, -v)$). These unknowns u, v can be computed in dependency of z from the following two equations, which arise from applying twice the *projection theorem*; i.e.

$$(D_0 - A_0)\mathbf{v}(A_0) = (D_0 - A_0)\mathbf{v}(D_0), \quad (D_0 - B_0)\mathbf{v}(B_0) = (D_0 - B_0)\mathbf{v}(D_0). \tag{13}$$

This already determines the infinitesimal motion up to the non-zero factor z .

5.4 Additional information

Crease patterns. The crease patterns of the structures displayed in Figs. 5a and 6a are given in Fig. 8. Note that for $n = 3$ the materialization of the faces α and β can be omitted as they are triangles.

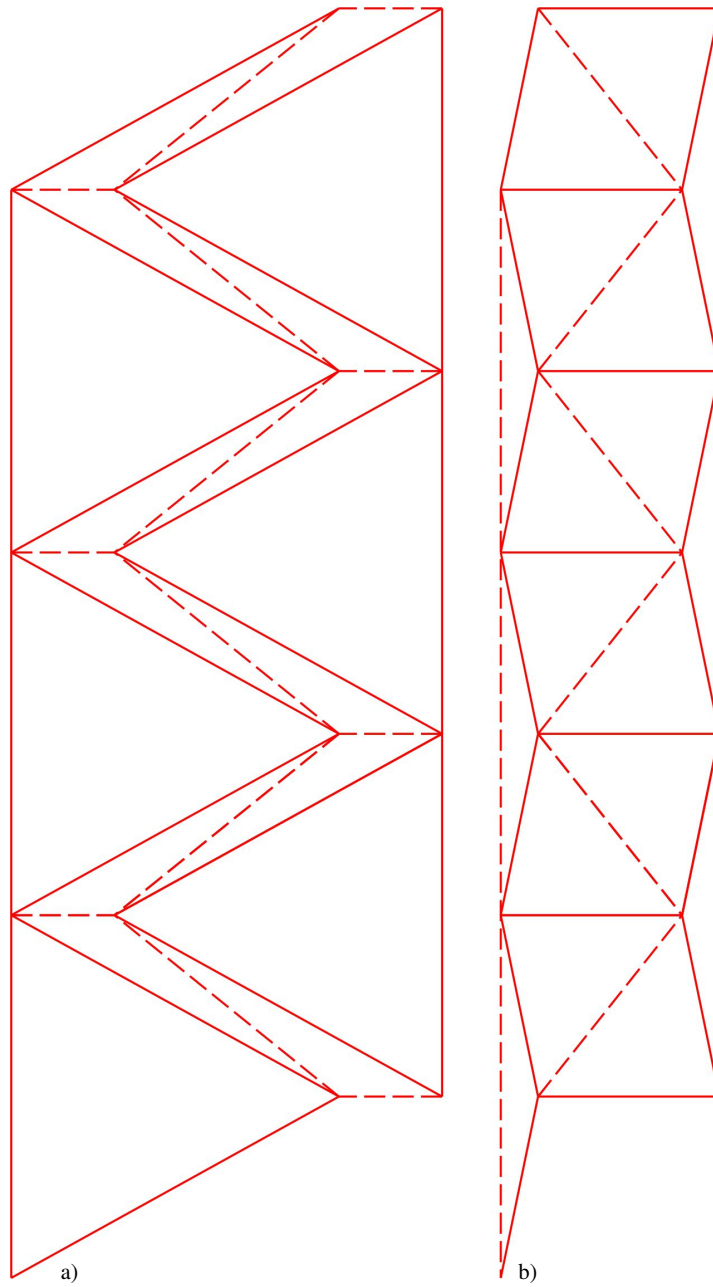


Fig. 8 (a) Crease pattern of the snapping structure displayed in Fig. 5a, where the mountain folds are solid and the valley folds are dashed with respect to the closed state. (b) Crease pattern of the shaky structure displayed in Fig. 6a, where the folds are marked in the same way.

Additional graphs. In the following we give some additional information on the families of snapping sandglasses (for $n = 3, \dots, 6$) computed in Section 3. The change of the height and the waist radius between the closed state and the open one relative to the radius of the n -gons in α and β , respectively, is displayed in Fig. 9a,b. The increase of the volume during the snap relative to the volume of the closed state is plotted in Fig. 9c. This change in volume confirms that there does not exist a continuous isometric deformation between the closed and open state due to the *Bellows conjecture*.

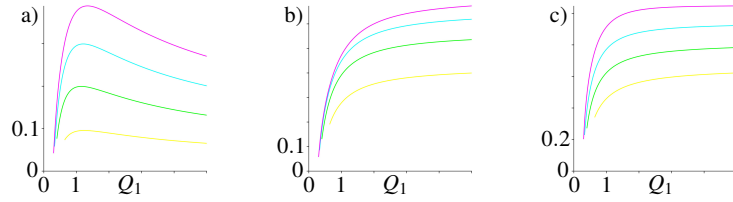


Fig. 9 The change of the height (a), the waist radius (b) and the volume (c) during the snap, where the same color-coding is used as in Fig. 4.